



Aalto University
School of Science
and Technology



Industrial systems

Environment-assisted cracking and hot cracking susceptibility of nickel-base alloy weld metals

<http://www.vtt.fi/inf/pdf/tiedotteet/2011/T2582.pdf>

Hannu Hänninen, Anssi Brederholm, Tapio Saukkonen and Mykola Ivanchenko
Aalto University School of Engineering

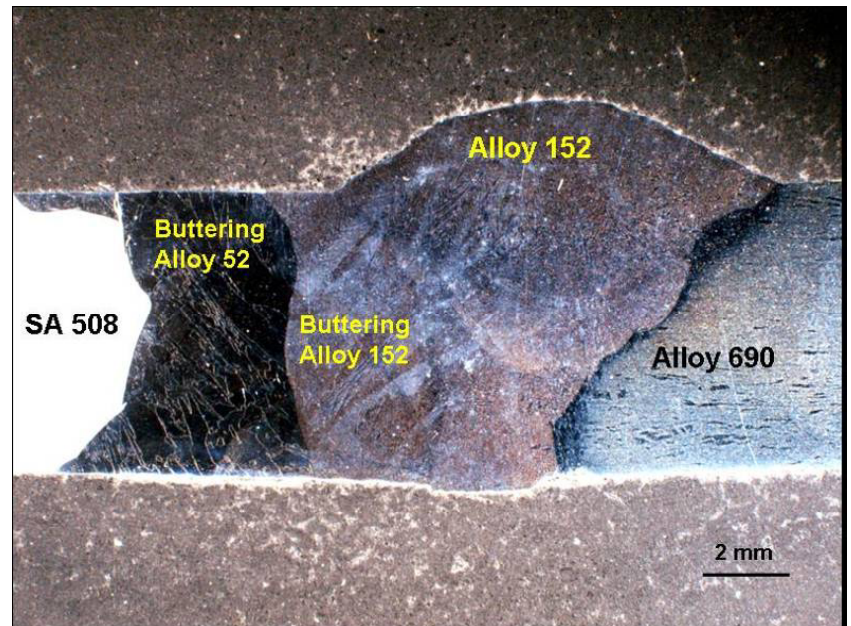
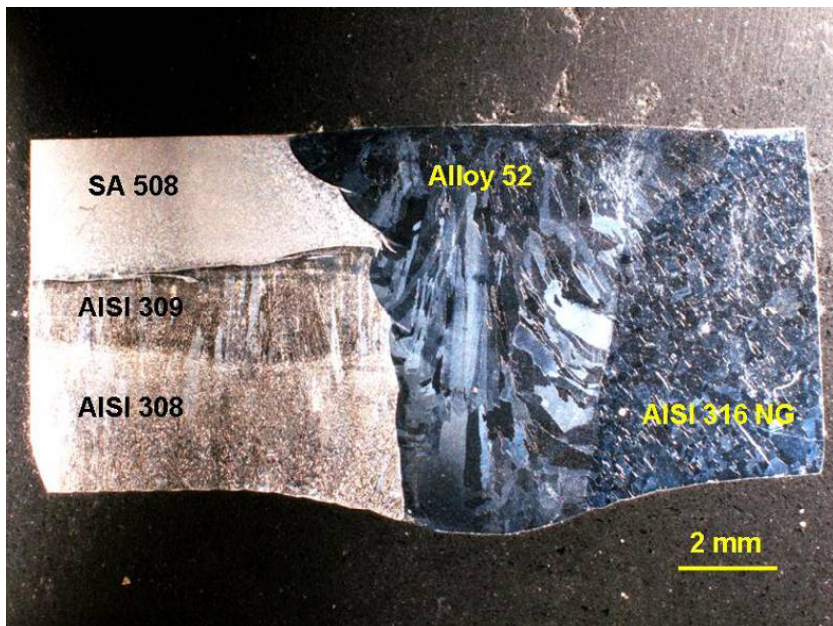
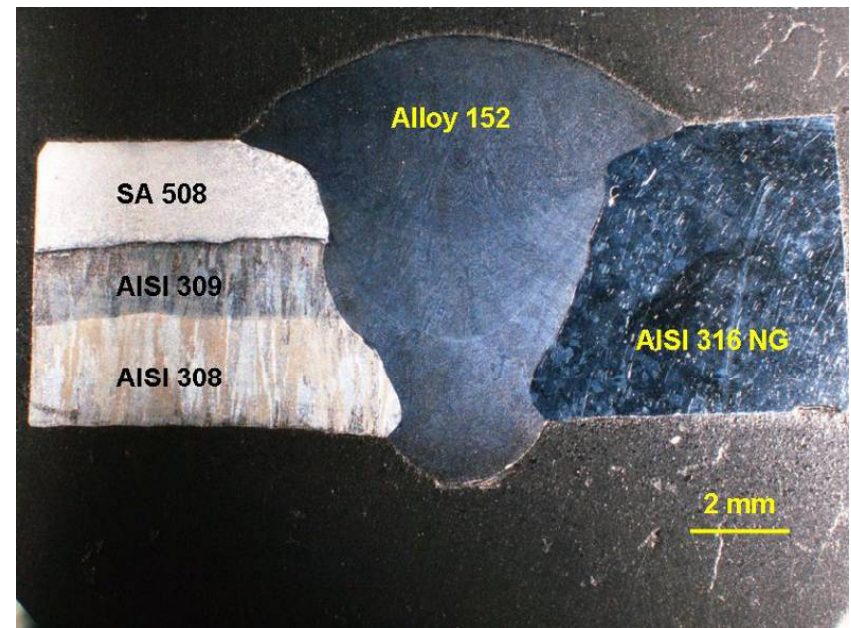
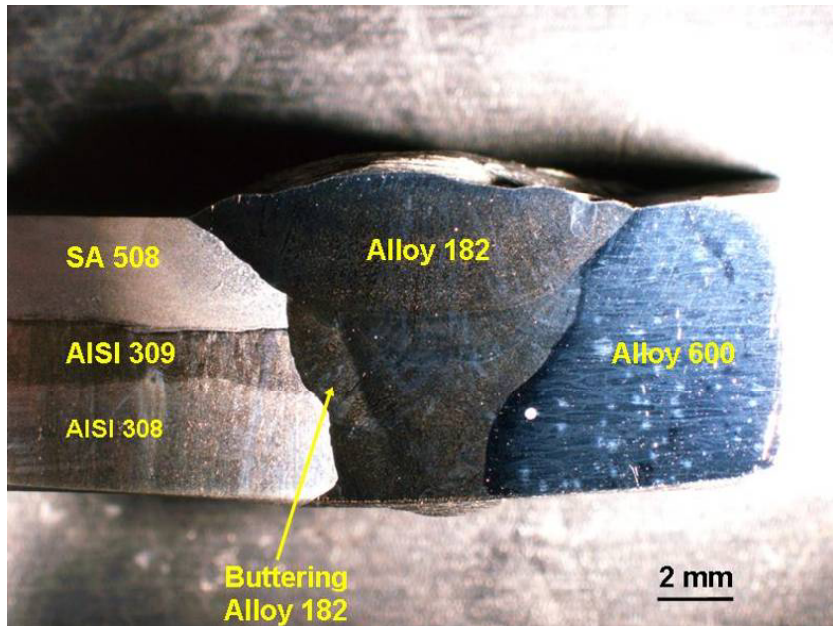
Aki Toivonen, Wade Karlsen, Ulla Ehrnstén and Pertti Aaltonen
VTT Technical Research Centre of Finland

NRC-Industry 2011 Meeting on Alloy 690 Research

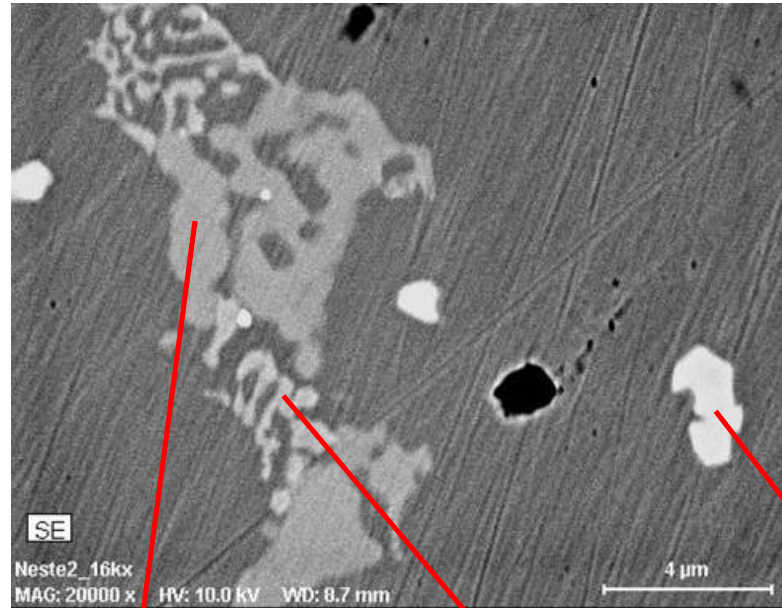
June 6 - 7, 2011

Rockville, Maryland

Dissimilar metal weld mock-ups



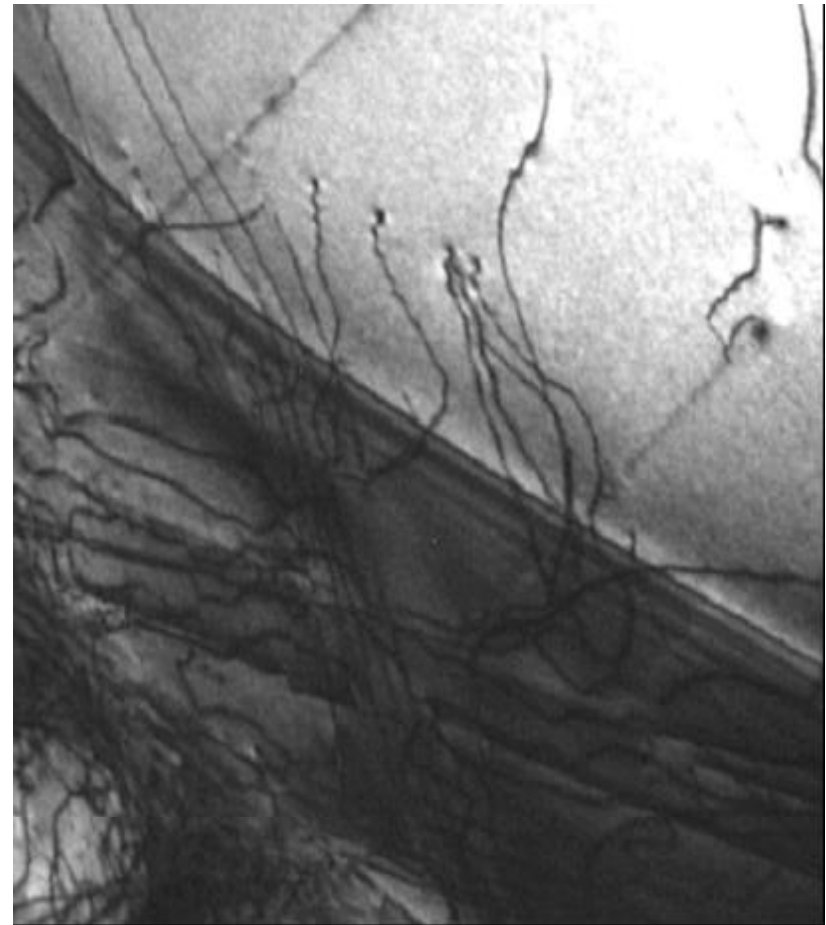
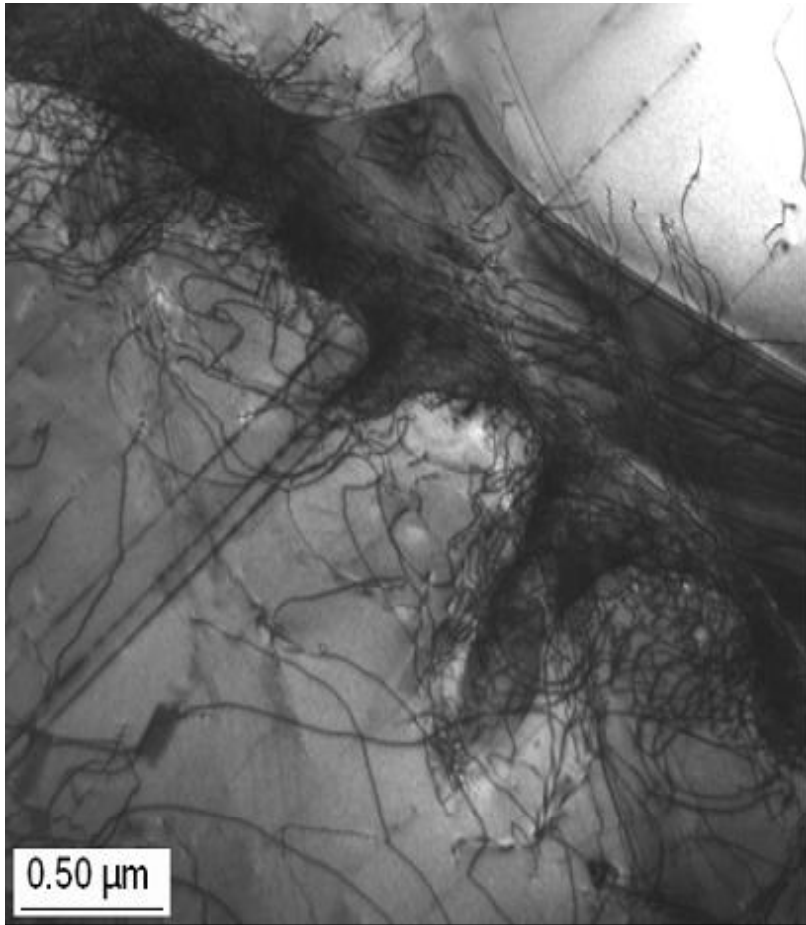
Hot crack tip chemistry



Element	Filler metal wt. %	Grey area wt. %	Enrichment vs. filler metal	Light white area wt. %	Enrichment vs. filler metal	White area wt. %	Enrichment vs. filler metal
Si	0,8	3,4	4,3	6,5	8,1	0	0,0
P	0,01	1,3	130,0	1,3	130,0	0,2	20,0
Ti	0,1	0,04	0,4	0,7	7,0	2,8	28,0
Cr	15,7	5,4	0,3	4,9	0,3	1,4	0,1
Mn	6,5	17,7	2,7	11,8	1,8	1,1	0,2
Fe	6,7	4,7	0,7	4,9	0,7	1,5	0,2
Ni	68	51,4	0,8	49,4	0,7	0	0,0
Nb	1,8	15,2	8,4	20,6	11,4	89,6	49,8

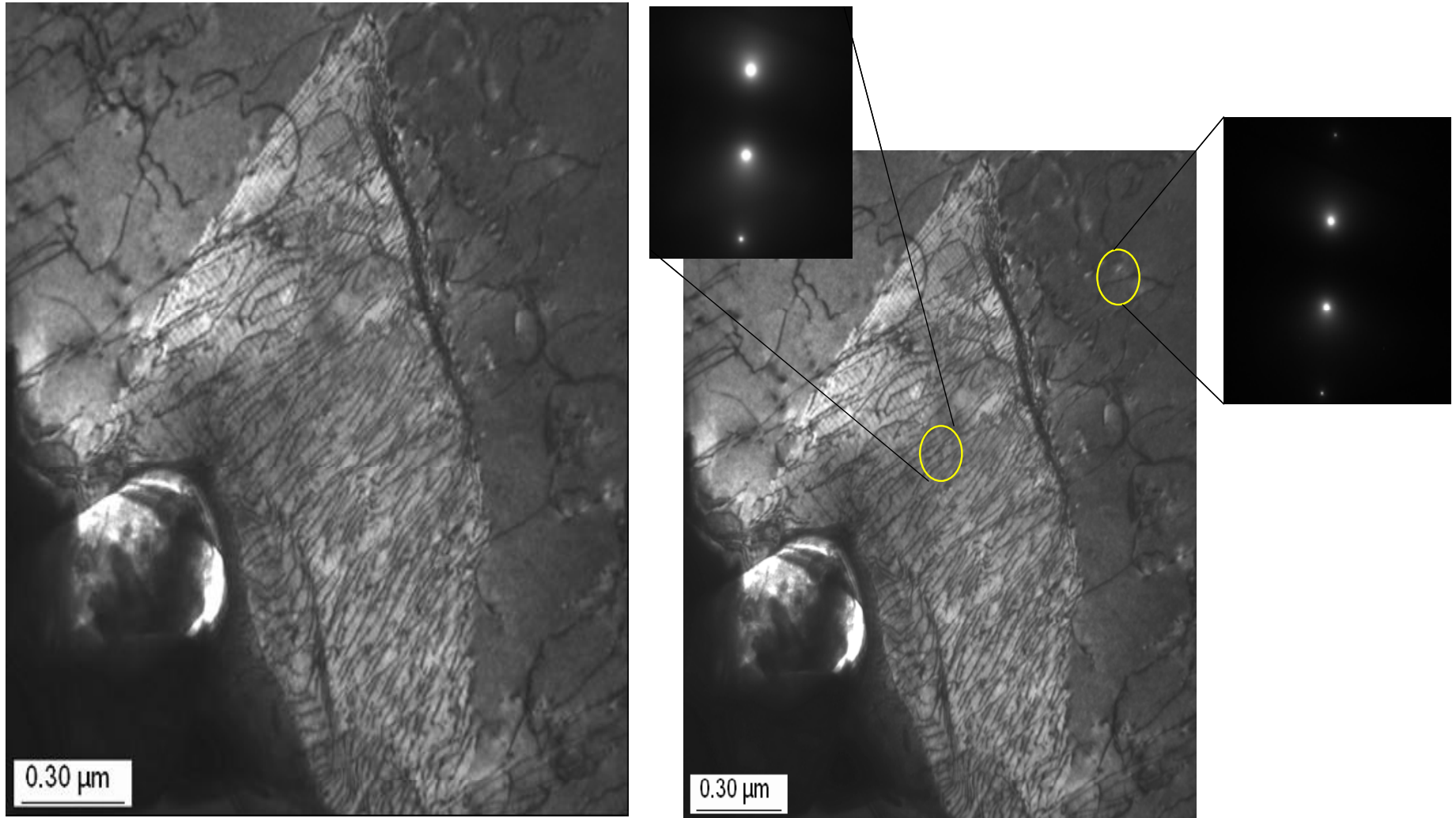
SEM image and EDS analyses of the white and grey phase in Alloy 182 weld showing Nb, Si, Mn and P enrichment and Nb-rich particles, Nb(C, N).

Hot crack tip ATEM



Diffuse dendrite boundary ahead of the hot crack tip shows marked compositional changes but no crystallographic lattice differences. The boundaries are distinguishable due to a thickness variation between the boundary region and the matrix. Dislocations are common to both matrix and the boundary region so they share their crystal lattice in spite of the Nb enrichment.

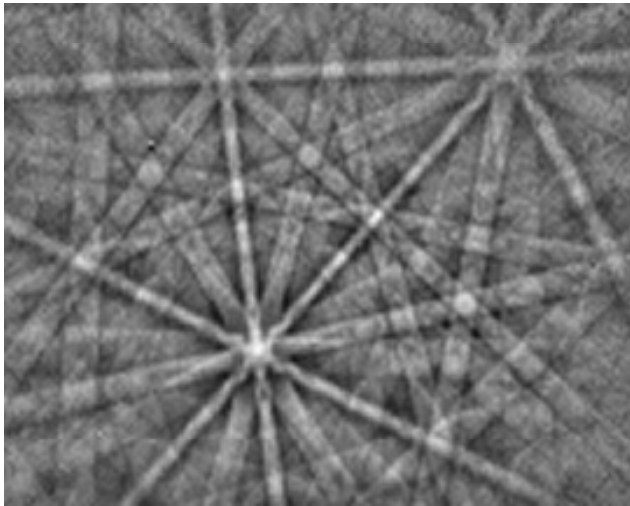
Hot crack tip ATEM



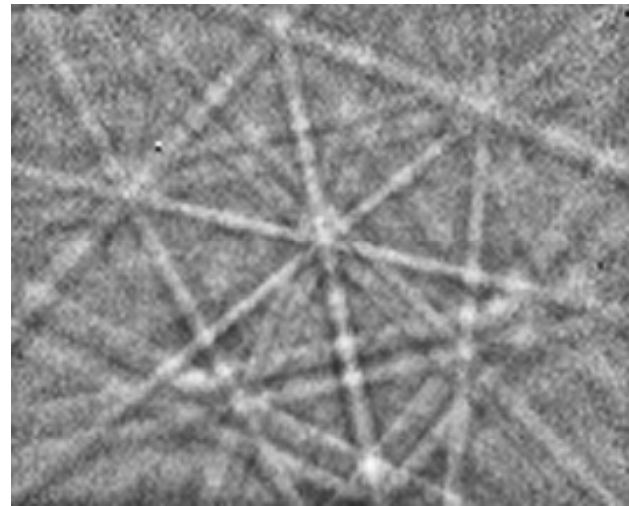
Eutectic regions have a high dislocation density and they show the same diffraction pattern with the matrix.

Laves phase EBSD

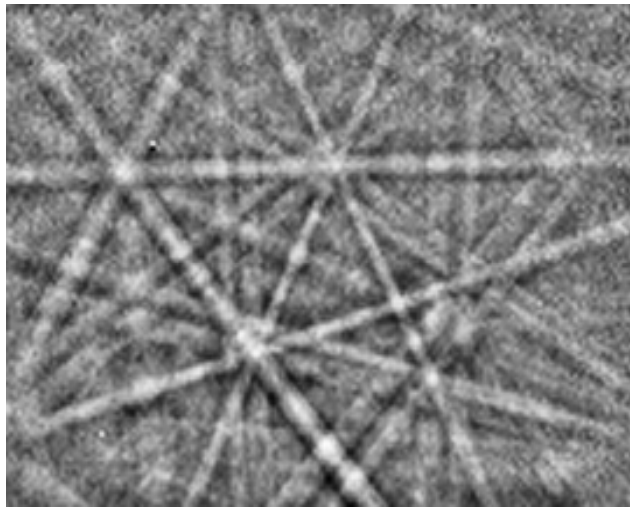
a)



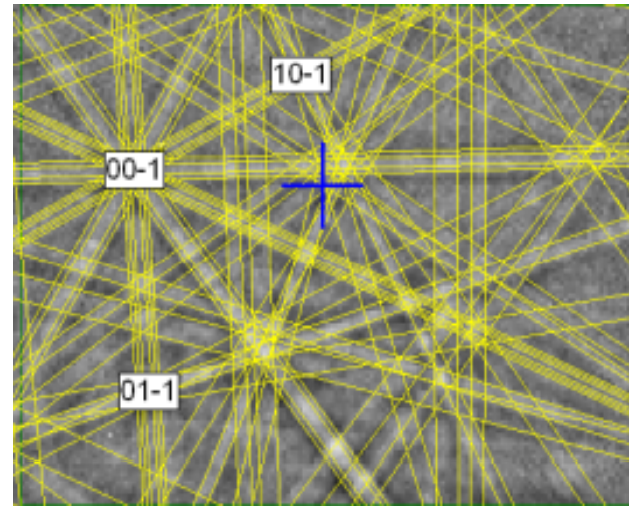
b)



c)

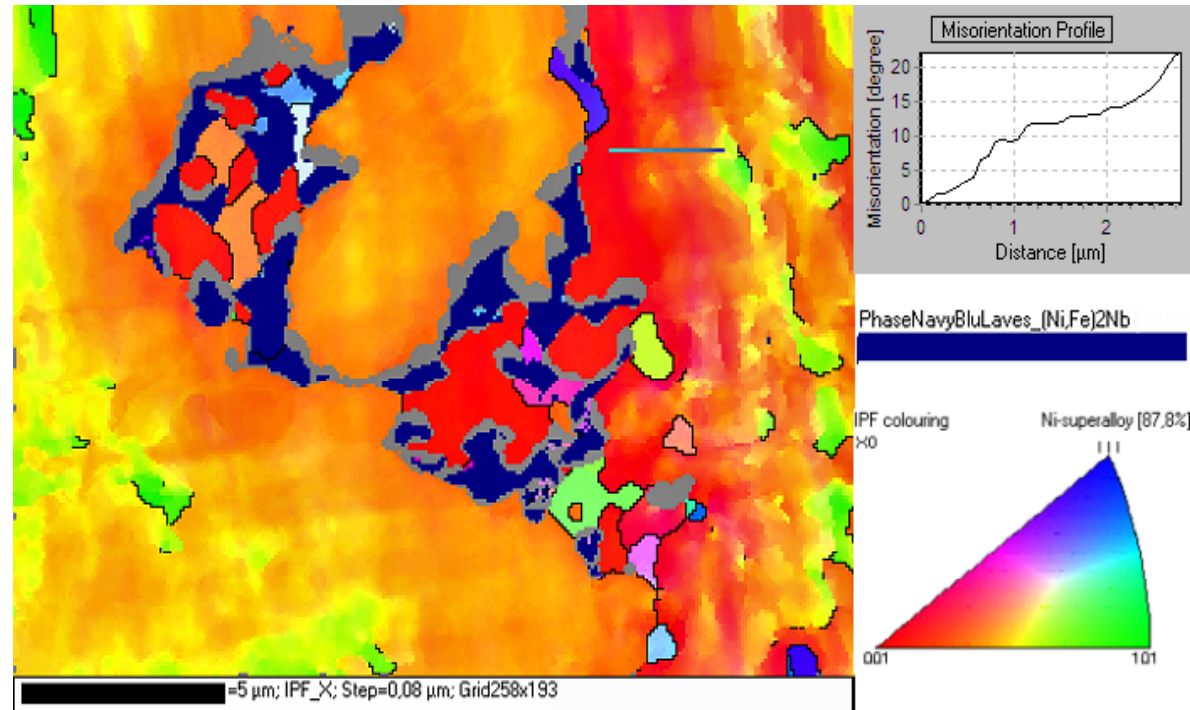
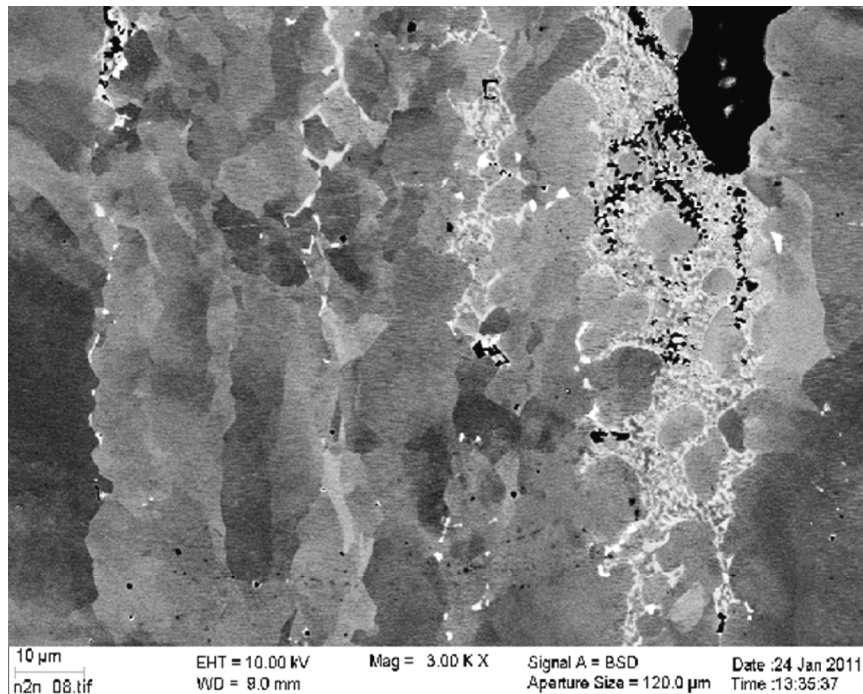


d)



Laves phase confirmation with EBSD for Alloy 182 hot crack tip. a) A typical EBSD pattern of the base material. b) An EBSD pattern of the white phase. c) Another EBSD pattern of the white phase. d) The solution with the formed Laves phase simulation.

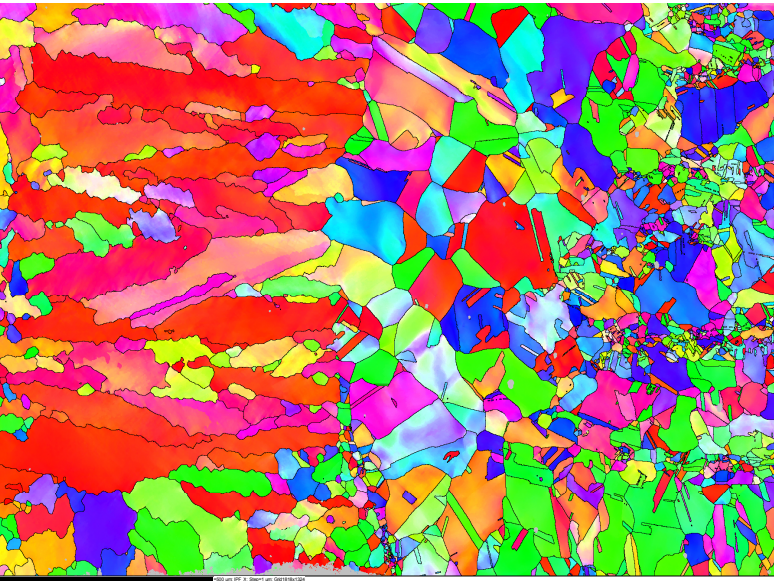
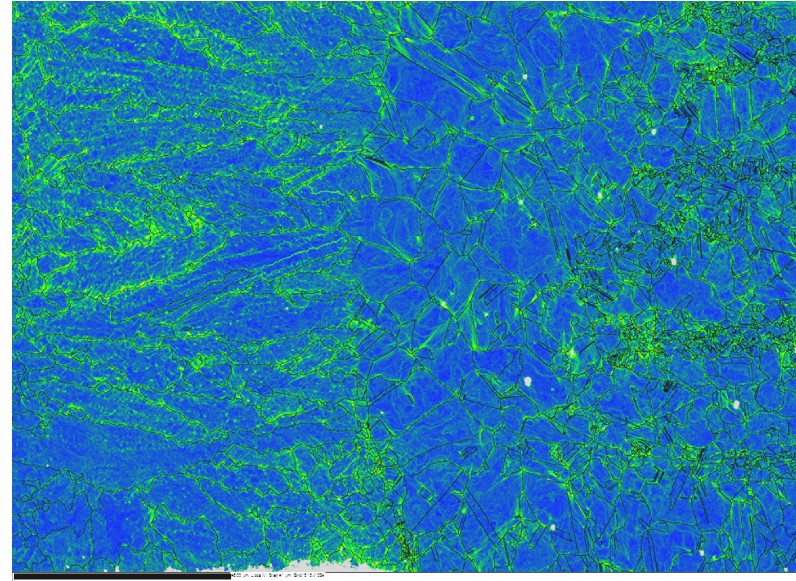
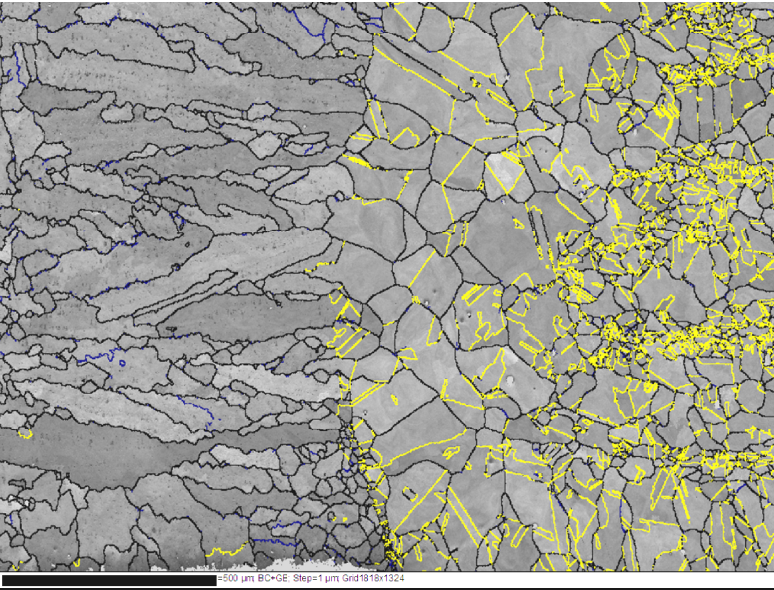
Laves phase



A channelling contrast backscattered image of an area with a large quantity of Laves phase. The clear cell structure in the base material between the Laves phase strings indicates a high degree of deformation in the base material close to the Laves phase.

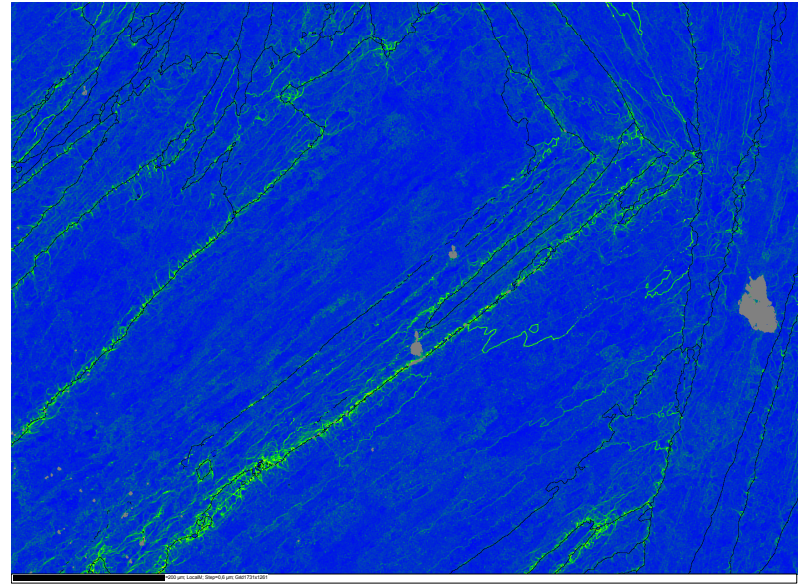
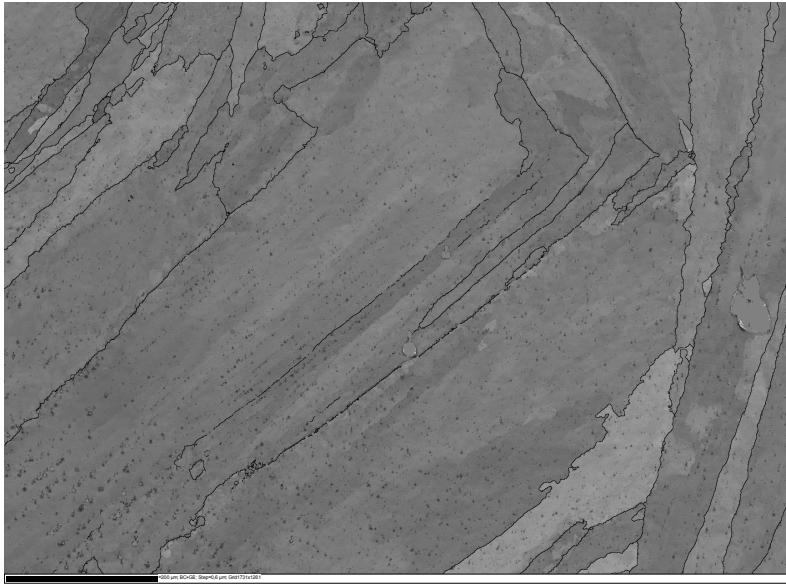
Inverse pole figure map of the base material with respect to x-direction and the Laves phase shown dark blue. The grain boundaries are marked by black lines. The misorientation line profile marked in the map shows a high degree of lattice rotation in the base material close to the Laves phase.

Alloy 182 EBSD

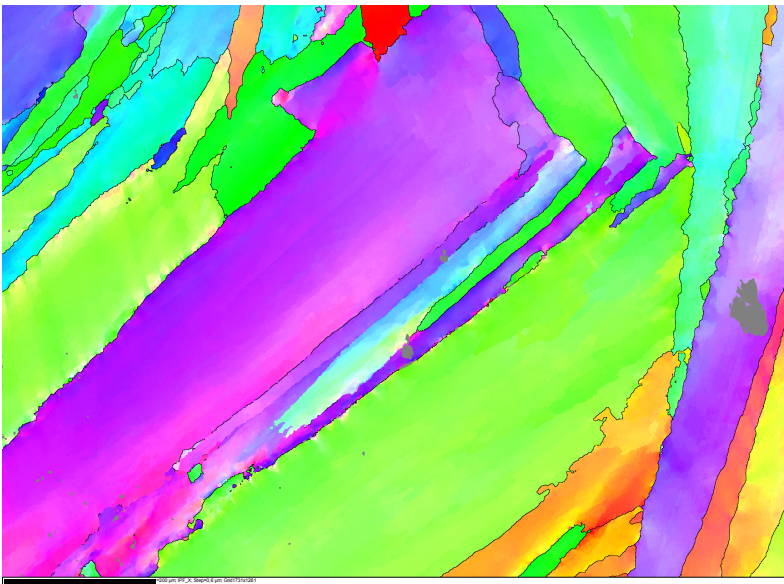


Microstructure of the mock-up TV DMW root, where Alloy 182 weld metal is in the middle, Alloy 600 safe end is on the right, and Alloy 182 buttering is on the left. The pattern quality map show the distribution of the grain size and grain form. The yellow lines in Alloy 600 show the twin boundaries inside the grains. The local misorientation map show clearly the local concentration of higher strain (green color) in the areas of dendrite boundaries. The inverse pole figure map shows also that inside the large grains, marked orientation differences are present.

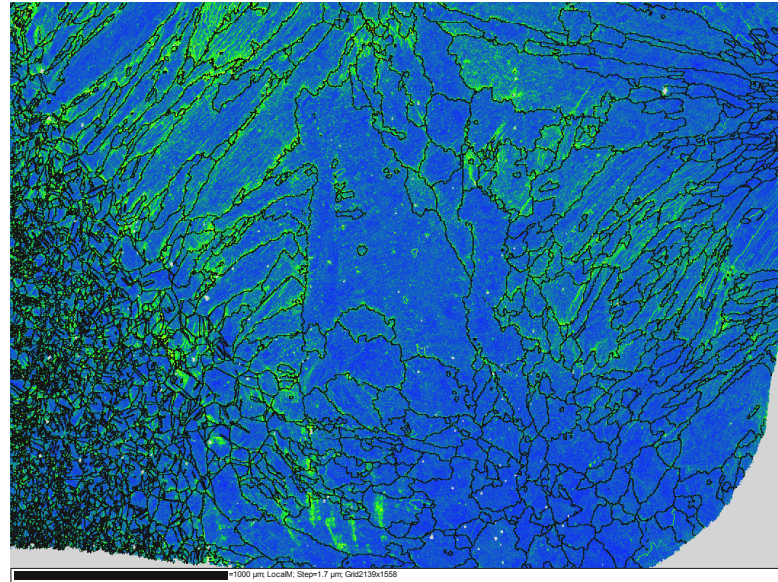
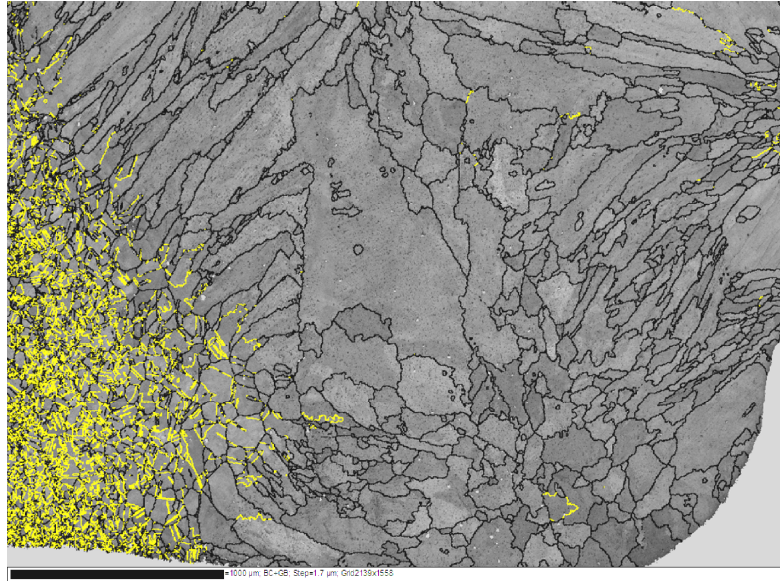
Alloy 182 weld metal EBSD



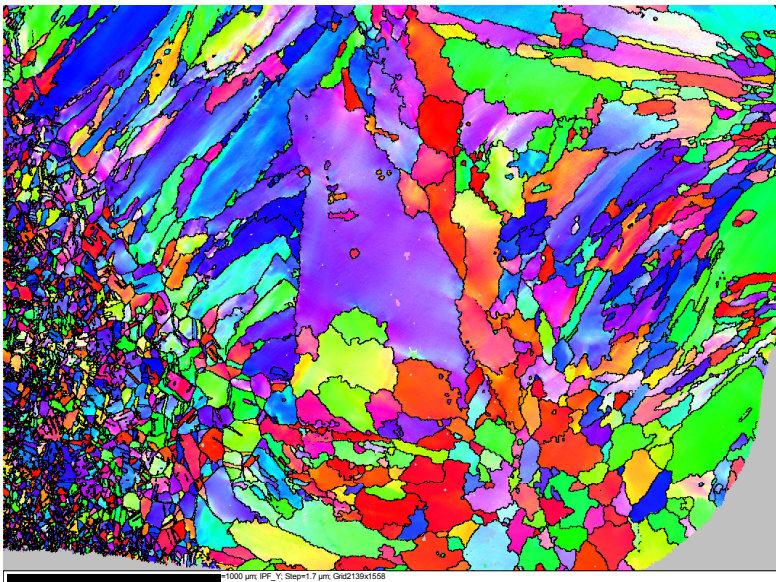
The pattern quality map shows the distribution of the grain size in the weld metal where very large grains are present. Inside the grains large orientation differences can be seen based on the variation of the grey color. The local misorientation map shows clearly the local concentration of higher strain (green color) close to the grain boundaries in the weld metal. The inverse pole figure map shows also that inside the large grains marked orientation differences are present.



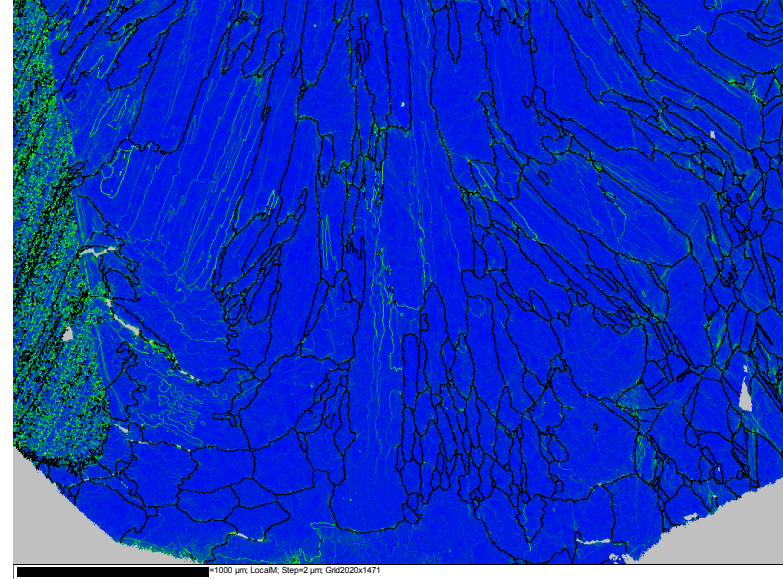
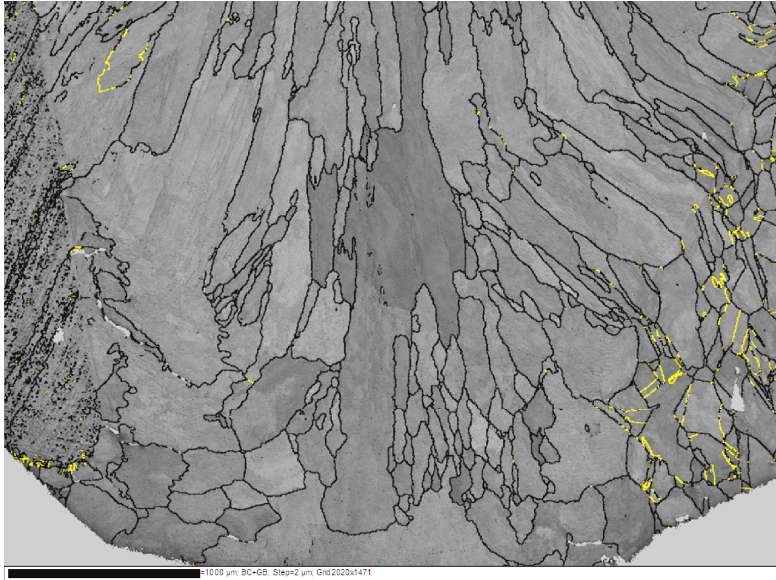
Alloy 152 weld root EBSD



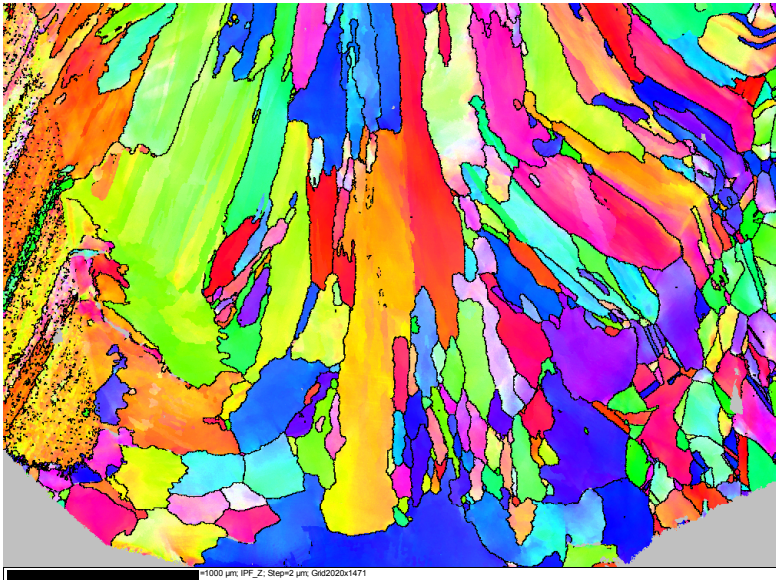
Microstructure of mock-up 1 weld root, where Alloy 152 weld metal is in the middle, AISI 316 NG safe end is on the left, and stainless steel cladding of the LAS is on the right side. The pattern quality map shows the distribution of the grain size and grain form. The yellow lines in AISI 316 NG show the twin boundaries inside the grains. The local misorientation map shows clearly the local concentration of higher strain (green color) in the areas of dendrite boundaries. The inverse pole figure map shows also that inside the grains marked orientation differences and small angle boundaries are present.



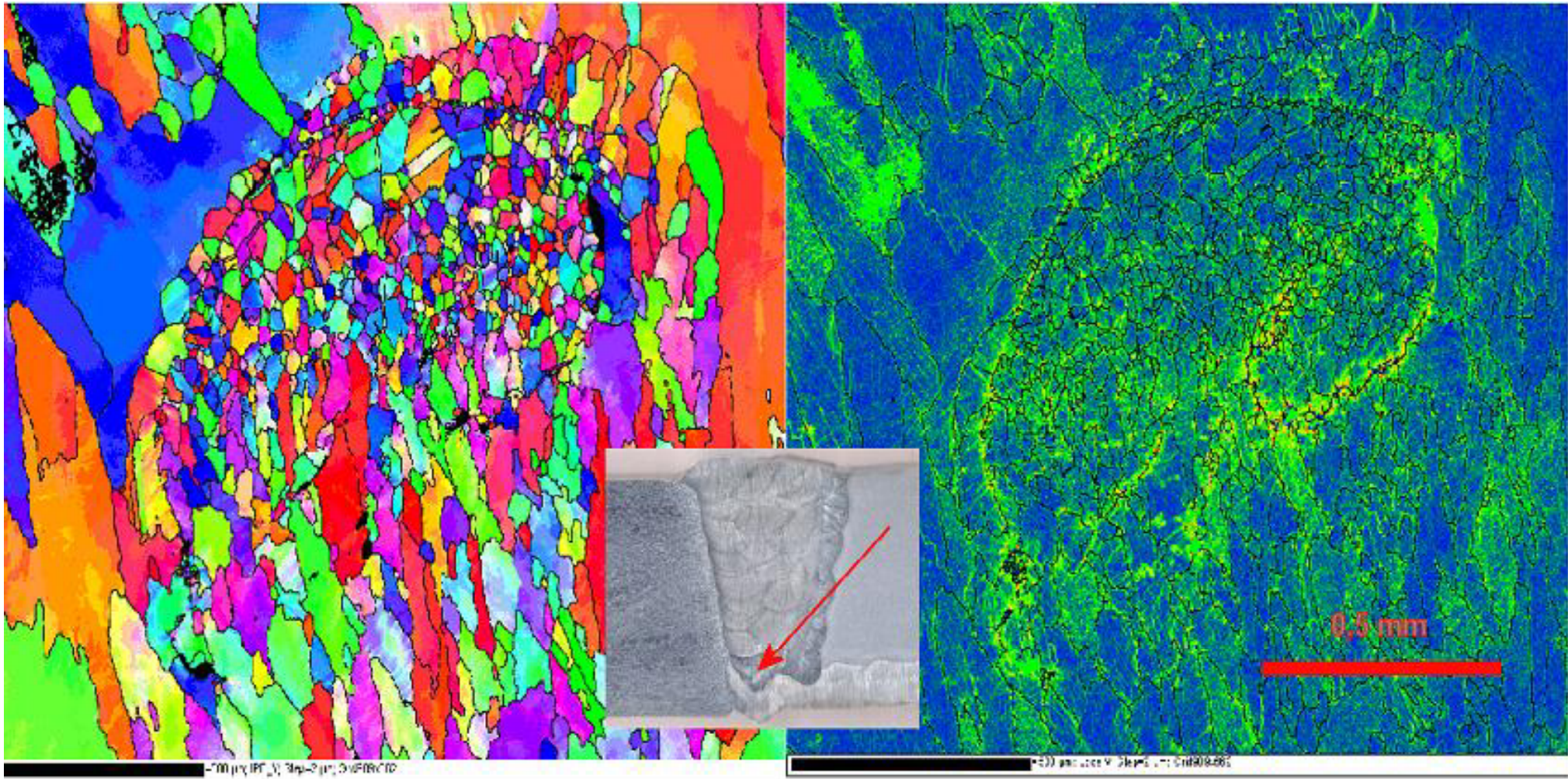
Alloy 52 weld root EBSD



Microstructure of mock-up 2 weld root where the Alloy 52 weld metal is in the middle, the AISI 316 NG safe end in on the right, and the stainless steel cladding of the LAS is on the left. The pattern quality map shows the distribution of the grain size and grain geometry. The yellow lines in AISI 316 NG show the twin boundaries inside the grains. The local misorientation map shows clearly the local concentration of higher strain (green color) in the HAZ in the stainless steel cladding. The inverse pole figure map shows that also within the grains marked orientation differences and small angle boundaries are present.

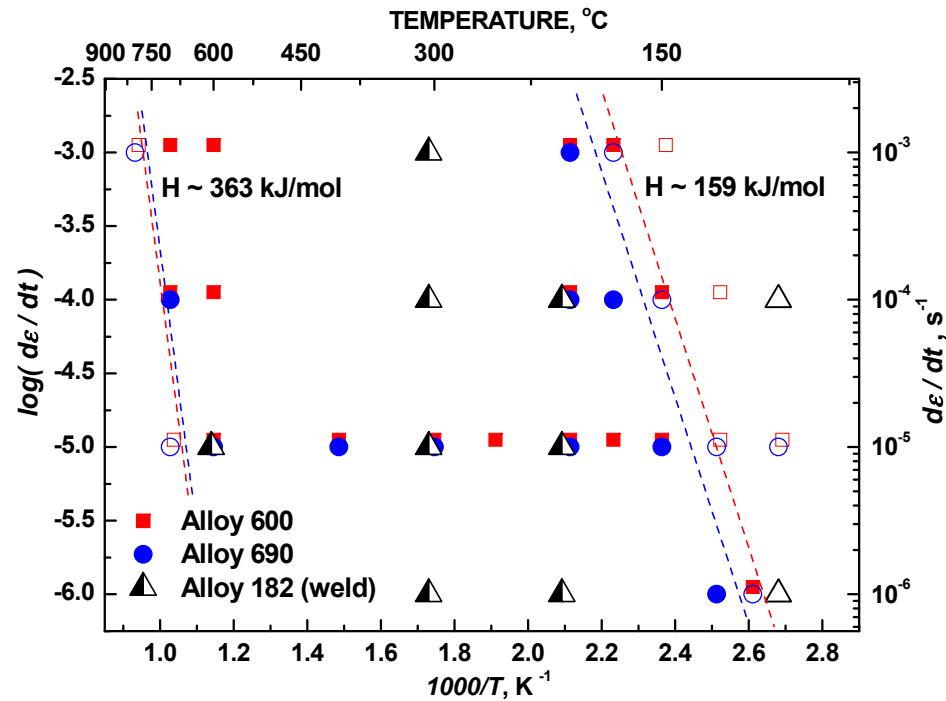
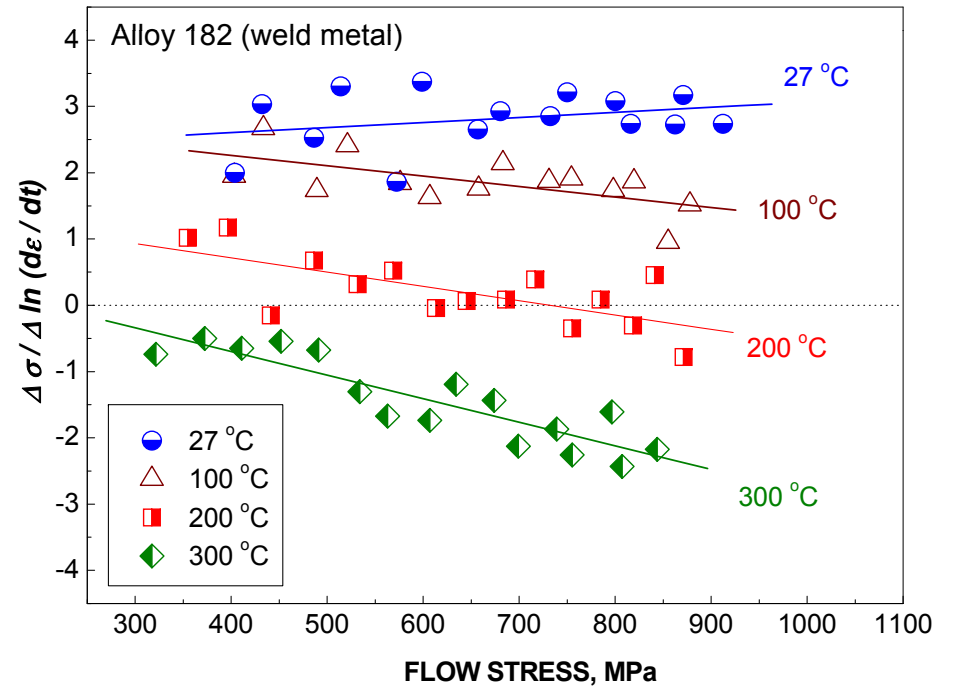
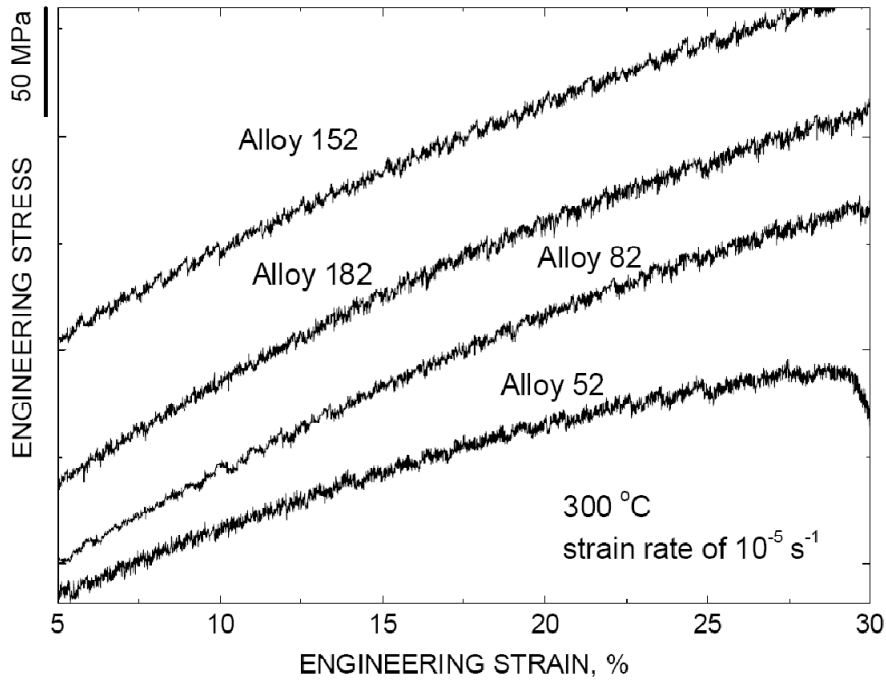


Weld defect EBSD



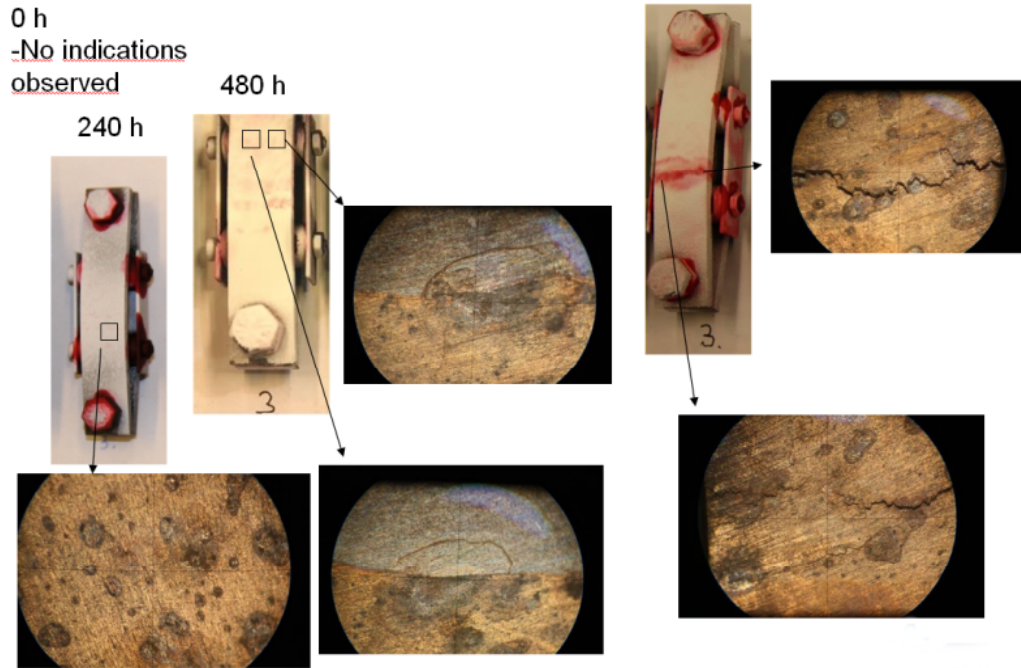
A weld defect in Alloy 82 weld metal mock-up DMW sample, where unmelted tip of the TIG filler metal wire is surrounded by the melted and solidified weld metal. On the left is an EBSD inverse pole figure map and on the right a local misorientation map. The location of the defect in the DMW is marked by an arrow.

Alloy 182 DSA

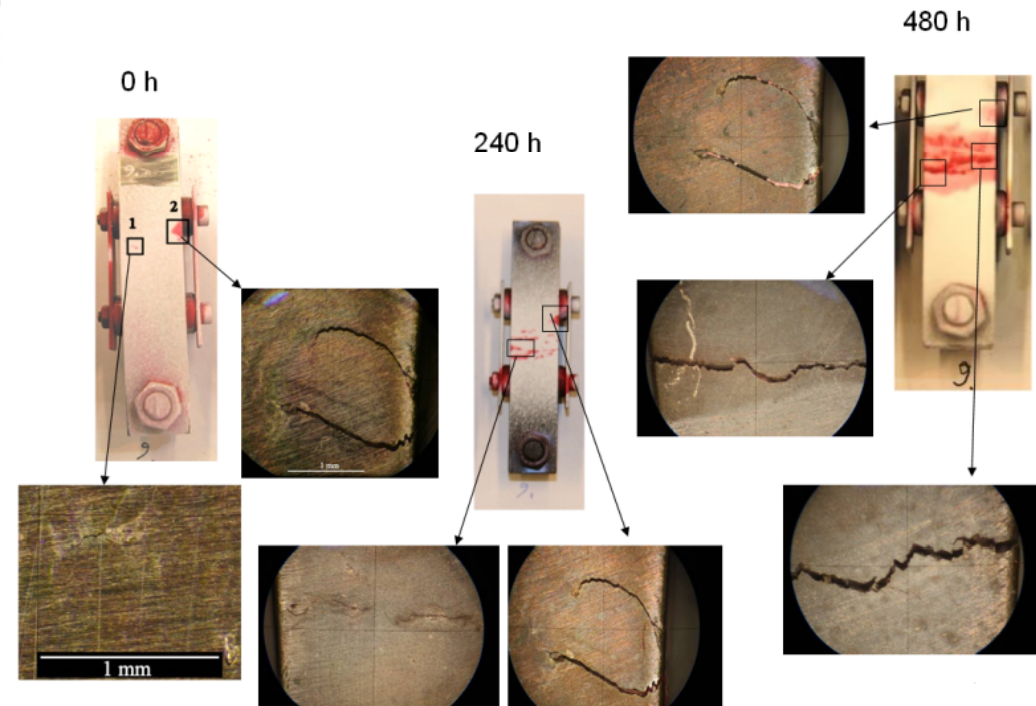


SCC in Alloy 182 and 82

Pure 182 (#3)



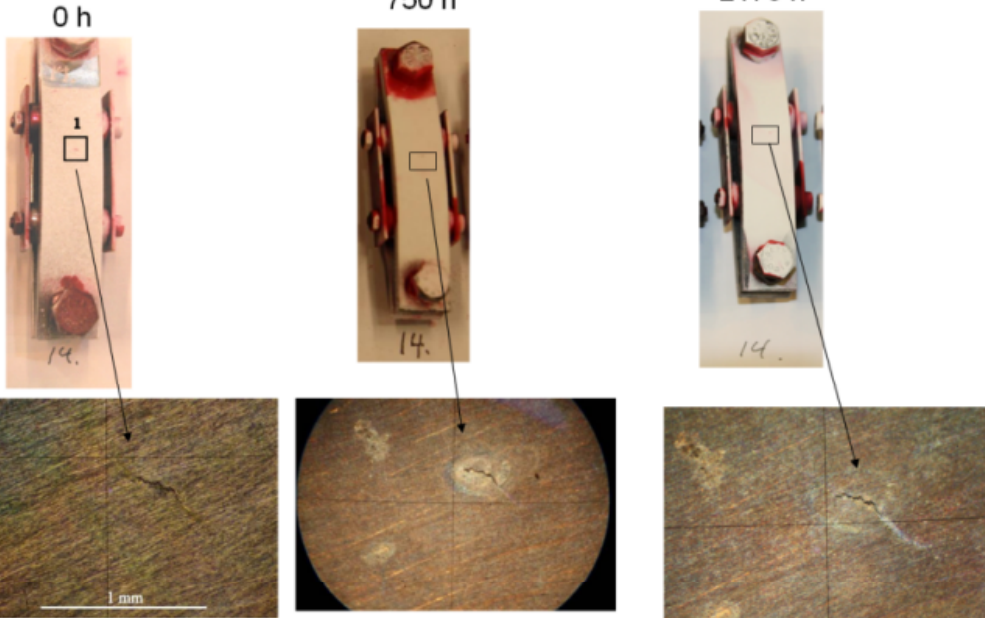
Pure Alloy 82 (#9)



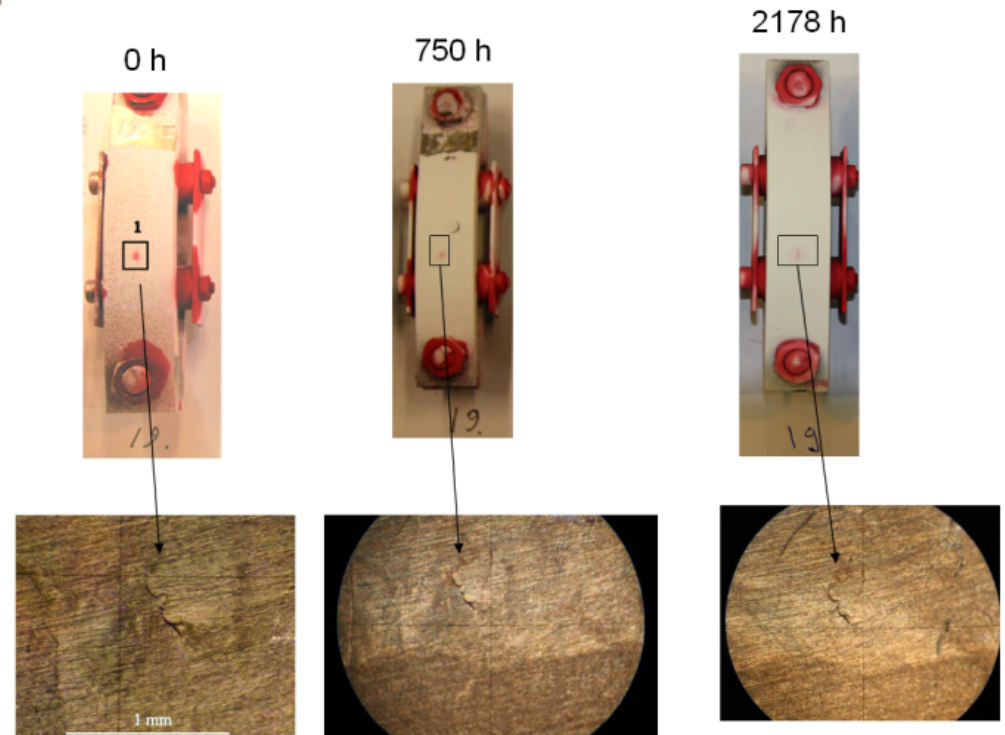
Neither in Alloy 182 nor in Alloy 82 the opened weld defects do not grow further and final fracture takes place in the middle of the specimens.

SCC in Alloy 152 ja 52

Pure 152 (#14)

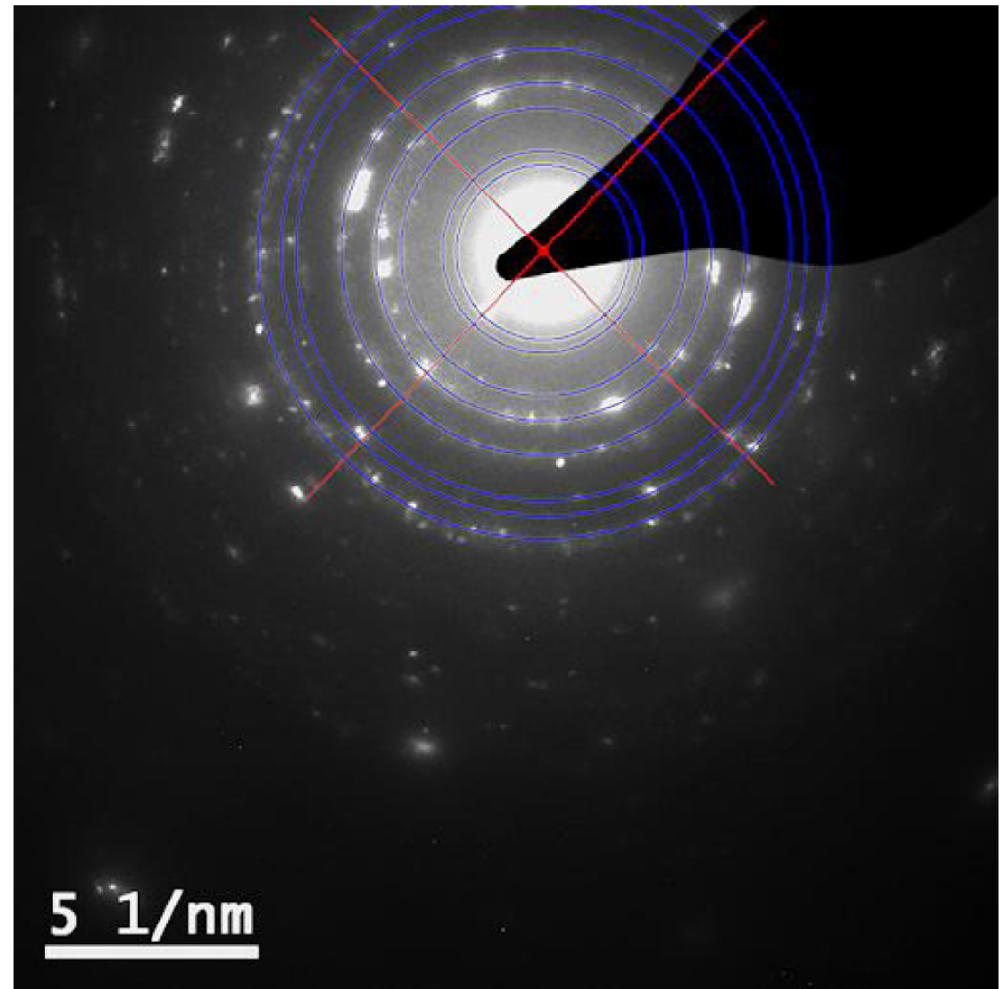
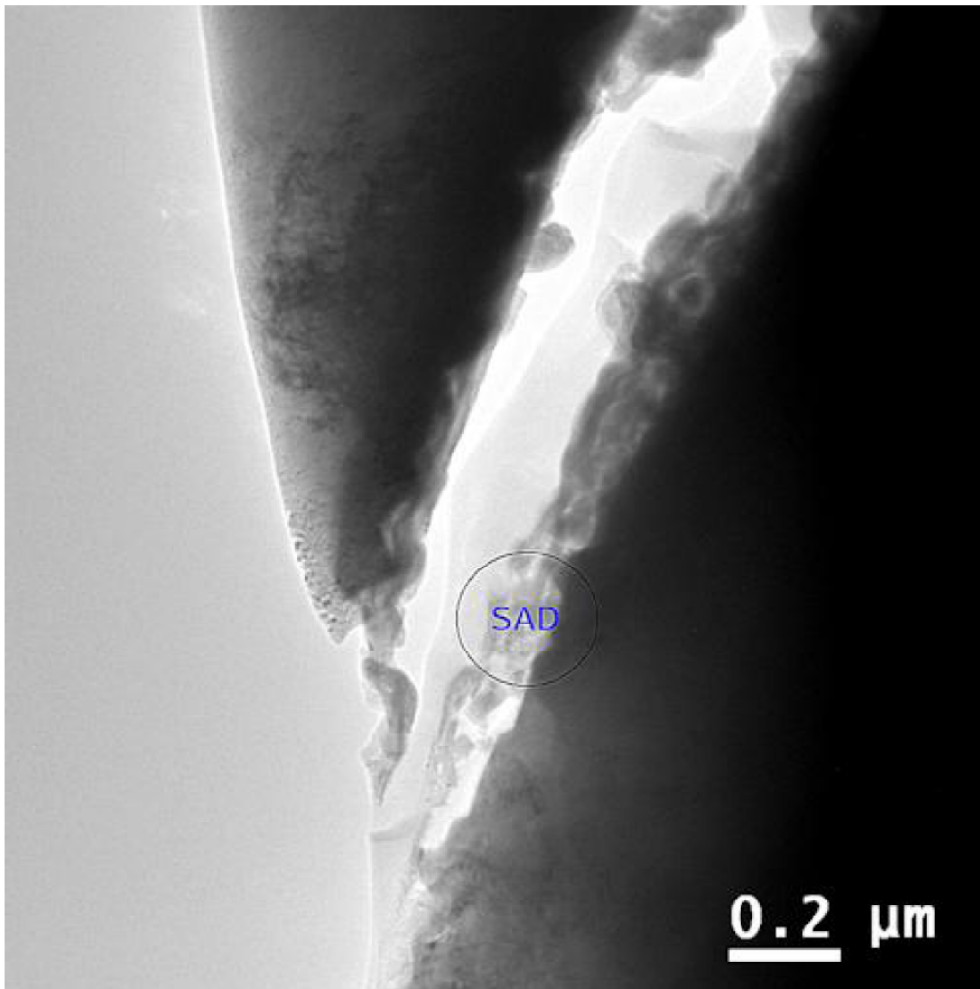


Pure 52 (#19)



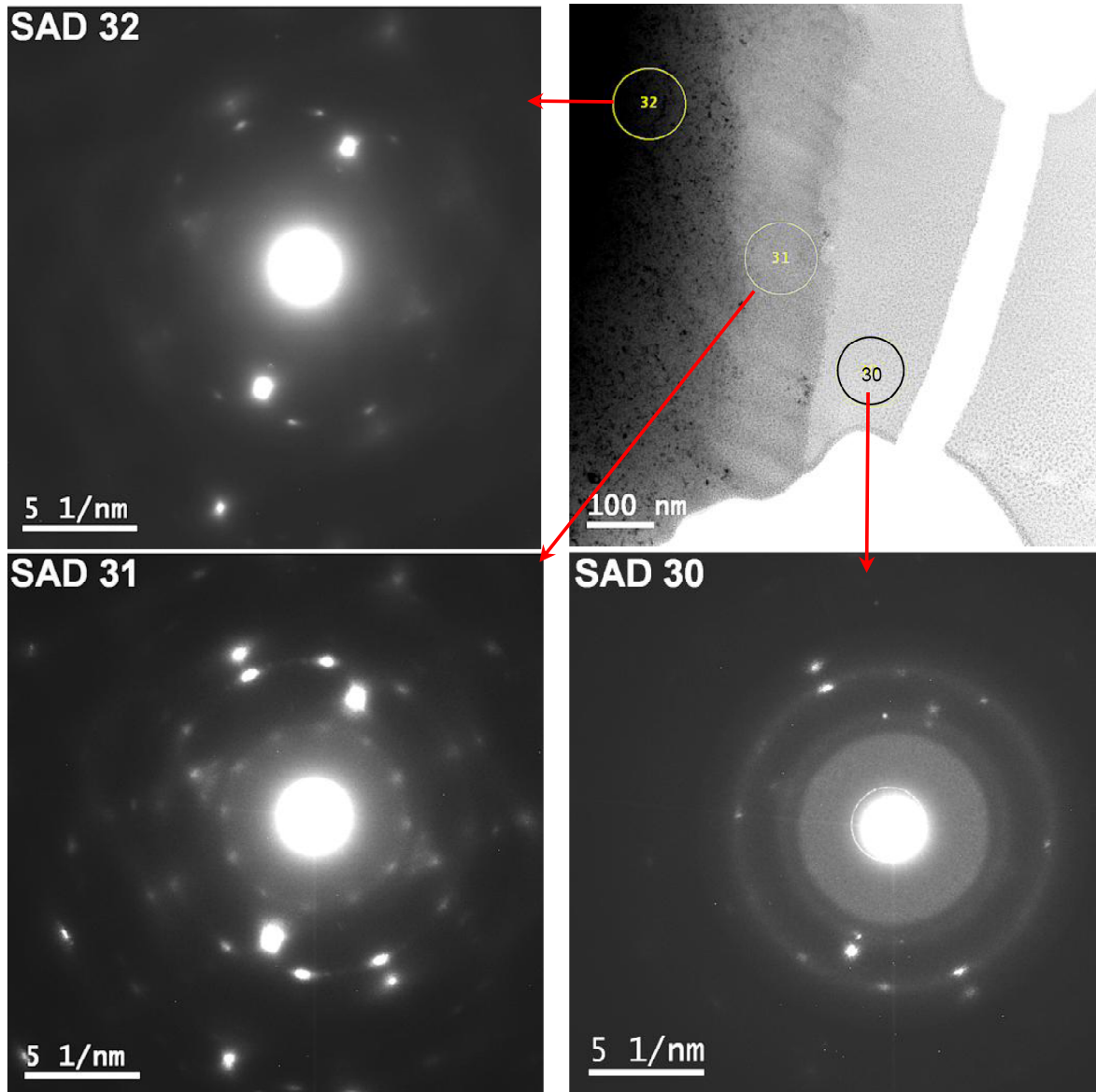
Neither Alloy 152 nor Alloy 52 did the opened small weld defects grow any further, nor did the alloys show any EAC crack initiation after any of the exposure times.

ATEM study of Alloy 182 crack



An example of a SAD ring pattern from the heterogeneous oxide at the crack wall of Crack C (location indicated in left hand image) suggested a diamond cubic structure similar to the idealized version of a spinel oxide having $a_0 = 8.36 \text{ \AA}$ (overlay rings in right hand image).

ATEM analysis of Alloy 182 crack tip oxide



SAD patterns of three oxide/matrix regions in Crack A, showing an apparent epitaxial oxide formation. SAD30 mostly indicates an almost amorphous NiO, with a couple of bright spots from the Ni alloy matrix. SAD31 shows much more predominant NiO with greater crystallinity indicated by the rings of equally spaced, but separate spots. The Ni alloy matrix spots are much more evident as well, and the two phases share an orientation relationship. Finally, SAD32 is comprised principally of the dominant pair of Ni alloy matrix spots, with only a minor presence of the larger ring of oxide spots, and no inner ring of spots.

Conclusions

- **Dissimilar metal weld joints of Ni-base weld metals show marked segregation in their microstructures, especially of Nb to the dendrite boundaries. In the Nb-bearing alloys eutectic Laves and Nb(C, N) phases form along the dendrite boundaries, and in Ti-alloyed Alloy 52 TiN(C) phase forms, respectively. These segregated structures and second phases play an important role in hot cracking, but were not found to enhance EAC in the doped steam test.**
- **The differences in the EAC susceptibility between different weld geometries and weld metals can be distinguished by the doped steam test method. Pure weld metals of Alloy 182 and 82 were clearly more susceptible to EAC than pure weld metals of Alloy 152 and 52, which did not show any crack initiation. The mock-up welds with diluted microstructures were less susceptible than the pure weld metals of Alloy 182 and 82. Aging at 420 °C for 2000 h did not seem to affect the cracking susceptibility in these test conditions.**
- **The accelerated doped steam test for Ni-base alloys results in a high acceleration factor for cracking, and because of the high temperature, the test conditions led to enhanced growth of oxide layer structures and clear separation of different phases.**
- **In the first test series, two main kinds of oxides were present on the fracture surfaces, containing mostly Ni, but arranged as a 30-50 nm thick Cr-rich inner layer showing spinel structure, and an outer layer having NiO type structure filling the rest of the crack.**

Conclusions

- **In the second test series, metallic Ni formed a continuous layer in the middle of the cracks surrounded by the Cr-rich oxide layer (locally also Nb-rich oxide may be present) in contact with the base material. On the outer surface islands of deposited Ni were also present.**
- **Cracking is consistent with a selective oxidation mechanism where vacancy injection into the base material is expected to enhance the creep rate at the crack tip. The mechanistic processes in steam and high temperature water are thought to be the same, at least for pure water.**
- **Dynamic strain aging is present in the studied weld metals of Alloy 182, 82, 152 and 52. Negative strain rate sensitivity observed for weld metal of Alloy 182 corresponds to tensile test temperatures and strain rates where serrated plastic flow was observed. Appearance of DSA manifested by serrated flow in weld metal of Alloy 182 fits well with the previously obtained map of the DSA appearance for the base materials of Alloy 600 and 690. Internal friction studies did not reveal any detectable IF peak attributed to free interstitial carbon or nitrogen atoms in FCC lattice of the studied weld metals in the same manner as it has earlier been reported for base material of Alloy 690.**
- **Specimens containing small weld defects or hot cracks did not show any crack extension in the doped steam test, either in pure weld metal samples or in mock-up samples after 2178 h. Also the hot crack surfaces showed little oxidation and no selective oxidation processes were observed on the hot crack fracture surfaces as compared to the fracture surfaces of the EAC cracks in the same exposure conditions. This indicates that the local microchemistry and microstructures on the dendrite boundaries ahead of the hot crack tips are not inherently susceptible to EAC.**